Frontiers in Earth Science

TYPE Original Research
PUBLISHED 05 April 2024
DOI 10.3389/feart.2024.1370992

Check for updates

OPEN ACCESS

EDITED BY
Paul Sestras,
Technical University of Cluj-Napoca, Romania

REVIEWED BY
Mohammad Azarafza,
University of Tabriz, Iran
Huajin Li,
Chengdu University, China
Sanda Rosca,
Babeş-Bolyai University, Romania

*CORRESPONDENCE
Chong Xu,
xc11111111@126.com

RECEIVED 15 January 2024
ACCEPTED 19 March 2024
PUBLISHED 05 April 2024

CITATION
Li T, Xu C, Li L and Xu J (2024), The landslide traces inventory in the transition zone between the Qinghai-Tibet Plateau and the Loess Plateau: a case study of Jianzha County, China.
Front. Earth Sci. 12:1370992.
doi: 10.3389/feart.2024.1370992

The landslide traces inventory in the transition zone between the Qinghai-Tibet Plateau and the Loess Plateau: a case study of Jianzha County, China

Tao Li[1,2], Chong Xu[1,2]*, Lei Li[3] and Jixiang Xu[4]

[1]National Institute of Natural Hazards, Ministry of Emergency Management of China, Beijing, China, [2]Key Laboratory of Compound and Chained Natural Hazards Dynamics, Ministry of Emergency Management of China, Beijing, China, [3]Key Laboratory of Shale Gas and Geoengineering, Institute of Geology and Geophysics, Chinese Academy of Sciences, Beijing, China, [4]Institute of Geology, China Earthquake Administration, Beijing, China

The upper reaches of the Yellow River in China, influenced by erosion of the Yellow River and tectonic activities, are prone to landslides. Therefore, it is necessary to investigate the existing landslide traces. Based on visual interpretation on high-resolution satellite images and terrain data, supplemented and validated by existing landslide records, this paper prepared the most complete and detailed landslide traces inventory in Jianzha County, Huangnan Tibetan Autonomous Prefecture, Qinghai Province, to date. The results indicate that within the study area of 1714 km^2, there are at least 713 landslide traces, ranging in scale from 3,556 m^2 to 11.13 km^2, with a total area of 134.46 km^2. The total landslide area excluding the overlap area is 126.30 km^2. The overall landslide point density and area density in the study area are 0.42 km^{-2} and 7.37% respectively. The maximum point density and maximum area density of landslide traces in the area are as high as 5.69 km^{-2} and 98.0% respectively. The landslides are primarily distributed in the relatively low-elevation northeastern part of Jianzha County, characterized mainly by large-scale loess landslides, with 14 landslides exceeding 1×10^6 m^2. This inventory not only supplements the landslide trace data in the transition zone between the Qinghai-Tibet Plateau and the Loess Plateau, but also provides an important basis for subsequent landslide risk zoning, response to climate change, and landscape evolution. Additionally, it holds significant reference value for compiling landslide inventories in similar geological environments.

KEYWORDS

landslide traces inventory, upper reaches of the yellow river, loess landslides, Jianzha County, visual interpretation

1 Introduction

Worldwide, mass movements such as landslides are prevalent geological hazards, causing heavy casualties (Petley, 2012; Froude and Petley, 2018). As far as landslide hazards are concerned, China ranks among the regions with the very frequency of landslide hazards globally (Kirschbaum et al., 2015; Xu and Xu, 2021). According to statistics from 2004 to 2016, China experienced 463 fatal landslides not induced by earthquakes, resulting in 4,718 deaths and causing economic losses exceeding 900 million dollars (Zhang and Huang, 2018). Therefore, the prevention and control of landslide hazards is crucial for people's lives. As a key step in hazard prevention and mitigation, including the analysis of regional landslide distribution patterns, hazard assessments, and risk assessment, the construction of a regional landslide inventory is fundamental and essential. A complete and accurate inventory ensures the objectivity and precision of subsequent work (Xu, 2015; Piacentini et al., 2018).

In the construction of China's landslide traces inventory, many scholars have carried out a lot of work and made certain progress (Chen et al., 2016; Qiu et al., 2019; Zhao et al., 2019; Zhang et al., 2020). In northwestern China, Huang et al. (2022) compiled a landslide traces inventory for Hualong County, Qinghai Province, consisting of 3,517 landslides through visual interpretation of high-resolution optical images. Furthermore, an in-depth study on the spatial distribution patterns of landslides was conducted based on this inventory. In central China, Li et al. (2022a) primarily utilized visual interpretation, supplemented by existing literature and hazard records, to improve and supplement the landslide traces inventory for Baoji City, Shaanxi Province. The inventory contains a total of 3,422 landslides, providing foundational data for subsequent exploration of the distribution characteristics of large-scale landslides in the region. In the western part of the Qinghai-Tibet Plateau, Cui et al. (2023) employed the Google Earth platform and visual interpretation method to identify landslide traces in the Western Himalayan Syntaxis. They established a landslide traces inventory containing 7,947 landslides. This inventory serves as a support for subsequent landslide hazard assessments. Wu et al. (2016) collected landslide data based on aerial photographs at a scale of 1:50,000 under the conditions of existing data and field survey. They mapped 328 landslides in Gangu County, Gansu Province, providing a crucial foundation for subsequent research. Lan et al. (2004) combined aerial photographs, previous landslide investigation data, and on-site verification to compile a landslide inventory for the Xiaojiang River Basin, including 574 landslide records. They conducted spatial analysis and prediction of landslide based on this inventory. The landslide data sets constructed by these studies, supported by various methods, demonstrate the ability to facilitate subsequent study on landslide in terms of accuracy and completeness. Nevertheless, accurate and complete landslide trace data are still lacking for the entire region of China.

In studies covering Jianzha County, many scholars have carried out identification work on regional landslides, or conducted research on landslide failure patterns, InSAR deformation analysis, geomorphic effects, and other aspects based on landslide data (Ma et al., 2008; Guo et al., 2020a; Wang et al., 2022; Tu et al., 2023). Yin et al. (2014) primarily utilized visual interpretation to identify 508 landslides from Sigou Gorge to Lagan Gorge in the upper reaches of the Yellow River, with many landslides distributed in Jianzha County. Tu et al. (2023) conducted landslide detection in the upper reaches of the Yellow River based on InSAR technology, and carried out detailed deformation analysis of the Lijia Gorge landslides group in Jianzha County. Du et al. (2023) combined InSAR deformation monitoring and optical images to identify 597 landslides in the upper reaches of the Yellow River. Landslides are mainly distributed in Jianzha County and its surrounding areas. Wang et al. (2022) conducted deformation analysis on the Simencun landslide in Jianzha County to explore the relationship between the failure patterns before and after the landslide occurrence. Currently, although many studies have been carried out in Jianzha County based on landslide data. However, the landslide inventory maps produced do not cover the entire Jianzha County, or the landslide data are not complete and detailed enough. Therefore, by combining the visual interpretation of high-resolution optical images with the comparison of existing literature, this study compiled a landslide traces inventory for Jianzha County, Qinghai Province. Additionally, a spatial analysis was performed on the inventory. Finally, the completeness and importance of the landslide inventory are discussed.

2 Study area

Jianzha County has a total area of approximately 1714 km^2 and is located in the transitional zone from the upper reaches of the Yellow River on the northeastern edge of the Qinghai-Tibet Plateau to the Loess Plateau (Figure 1) (Ma et al., 2008). For a long time, the landscape evolution of this region has been influenced by the northeastward compression of the Qinghai-Tibet Plateau, resulting in the formation of basin and mountainous topography (Guo et al., 2020a; Peng et al., 2020). The overall terrain in the region is high in the southwest and low in the northeast. The northeastern part is the Qunke-Jianzha Basin, characterized by relatively low elevations and crossed by the main trunk of the Yellow River. On either side, there are two basins, namely, the Guide Basin and the Xunhua Basin. The Yellow River and its tributaries exert strong erosion and incision along the edges of the basins, with cutting depths exceeding 500 m. This has resulted in the formation of numerous erosion and accumulation terraces, as well as steep and rugged slopes, providing favorable conditions for landslide occurrence (Craddock et al., 2010; Guo et al., 2020a; Du et al., 2023).

The study area exhibits undulating and rugged topography with well-developed valleys and gullies. The surrounding active tectonics are developed, with the north part of the area having the Lajishanbeiyuan Fault (LJSBYF) and the Lijishannanyuan Fault (LJSNYF). The NWW-SEE trending Daotanghe-Linxia Fault (DTH-LXF) and NNW-SSE trending Riyueshan Fault (RYSF) pass through the study area. Tectonic activity and climate change contribute to the frequent geological hazards (Yin et al., 2014). The large, extra-large, and giant landslides in the region are typical and representative in China (Guo et al., 2020b; Yin et al., 2021). Some studies suggest that the tectonic uplift of the Qinghai-Tibet Plateau, as an internal dynamic factor, has led to the episodic incision of the Yellow River main and tributary channels, serving as the underlying cause for the formation of giant landslides (Li et al., 2011). As shown in Figure 1, there are several historical earthquakes with Ms greater than 5.0 around Jianzha County. The occurrence of landslides may be related to seismic activity or may be the result of landscape evolution, such as river erosion and high groundwater levels (Guo et al., 2016; Guo et al., 2018).

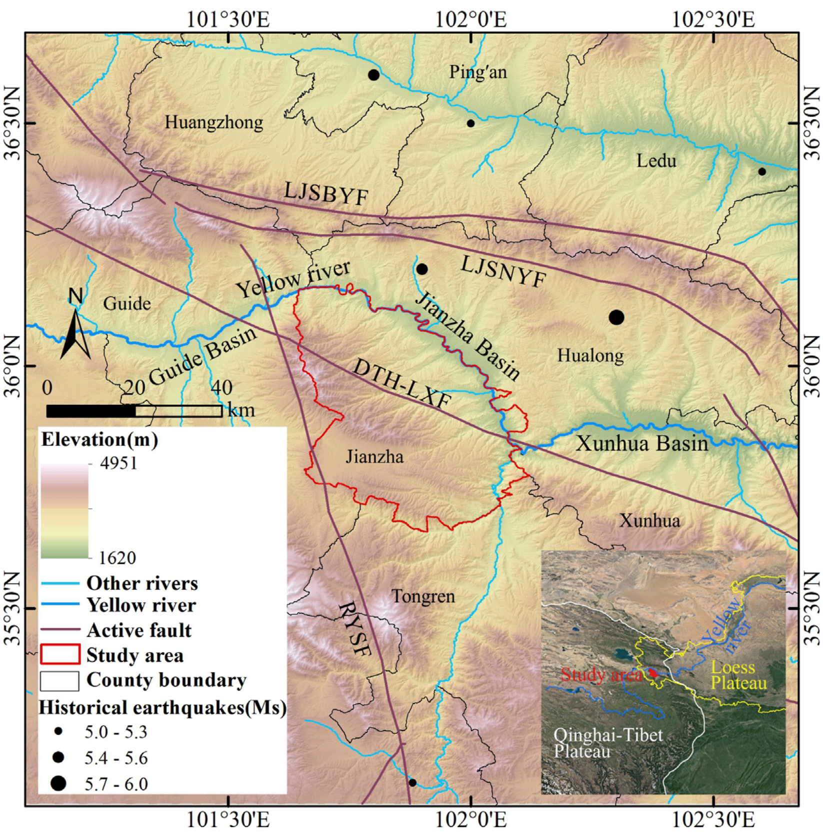

FIGURE 1
Location of the study area. Surface wave magnitude (Ms) is a measure of the strength of an earthquake, calculated from surface wave. The larger the value, the stronger the earthquake. Active fault data from Deng (2007).

3 Methods

With the advancement of remote sensing technology and improved transportation accessibility, the main methods for compiling regional landslide inventories currently include field investigation, visual interpretation of satellite images combined with computer, and automatic identification technology. Table 1 summarizes the advantages and disadvantages of the three landslide identification methods. Detailed field investigation can ensure high accuracy for landslide investigations in small-scale areas (Huangfu et al., 2021). However, for large-scale regional landslide investigations, the feasibility of extensive field investigation decreases. This is primarily due to the substantial cost and time required (Peng et al., 2016), as well as the difficulty in accessing rugged landslide sites. With the development of automatic identification technology, it has a significant advantage in quickly obtaining regional landslide data. However, its accuracy may be not very good (Fayne et al., 2019; Zhang et al., 2020; Piralilou et al., 2021; Vecchiotti et al., 2021; Milledge et al., 2022). Combining the strengths of both approaches, the human-computer interaction visual interpretation of satellite images has gradually become an important method for constructing landslide inventory (Xu et al., 2015; Shao et al., 2020; Li et al., 2021; Cui et al., 2022a). This approach requires interpreters to have certain professional background knowledge. Compared to detailed field survey, it sacrifices a small portion of accuracy but significantly improves the efficiency of constructing landslide inventory (Xu et al., 2014b; Cui et al., 2022b; Cui et al., 2022c).

This article primarily employed high-resolution optical images overlayed on terrain data for human-computer interactive visual interpretation, and combined existing landslide records in literature for validation and supplementation to construct a landslide traces inventory for Jianzha County. Google Earth Pro platform integrates a vast amount of high-resolution optical satellite image data and allows for the three-dimensional, multi-angle display of landscape by overlaying terrain data (Crosby et al., 2012; Rabby and Li, 2019). This provides extremely convenient conditions for landslide identification. Focusing on the Jianzha County, the image quality is exceptionally high, with 100% satellite image coverage and 0% cloud coverage. Therefore, we performed repetitive basic work on landslide interpretation based on the Google Earth Pro for inventory construction. First of all, the shape and boundary of the landslide can be easily determined based on the differences between the texture, tone, shadow and vegetation development on the satellite images and the surrounding environment, combined with terrain differences and multi-angle observation. Secondly, many existing literature findings on landslides in the region will be conducted to check and supplement the inventory for ensuring the completeness and objectivity. Because different landslides have different topographic and geomorphic characteristics, there is no

TABLE 1 Advantages and disadvantages of three landslide identification methods.

Methods	Advantages	Disadvantages	Scope of application
Detailed field investigation	Precision, accurate landslide parameter measurement	High cost, high time consumption, difficult to access in rugged terrain	High-precision landslide investigation in a small area with convenient transportation
Automatic identification technology	Low cost, less time consumption, rapid mapping, emergency response	Low accuracy, prone to omissions	Emergency response to landslides induced by earthquake or rainfall
human-computer interactive visual interpretation	Balancing efficiency and quality, high accuracy	Professional background required	Construction of inventories for large area event-based landslides and landslide traces

TABLE 2 Selected recorded landslides in Jianzha County.

No.	Name	Longitude	Latitude	Citation
1	Simencun Landslide	101.94°	36.04°	Wang et al. (2022)
2	Xiazangtan landslide	102.00°	35.98°	Guo et al. (2020b)
3	Lijia Gorge landslide group	101.75°	36.14°	Tu et al. (2023)
4	Kangyang landslide	101.96°	36.00°	Yin et al. (2013a)
5	Lannitan landslide	101.98°	36.00°	Yin et al. (2013a)
6	Tangse landslide	101.82°	36.09°	Yin et al. (2013b)
7	Quhetankou landslide	101.94°	36.01°	Yin et al. (2013b)
8	Gurisi landslide	102.02°	35.97°	Ma et al. (2008)

uniform standard applicable to the interpretation of all landslide traces. Here, some common landslide features used in landslide interpretation are listed: 1) Having an obvious armchair-shaped back wall and the phenomenon of double grooves homologous; 2) Depression in the source area, prominent topography in the accumulation area, accompanied by a distinct landslide boundary; 3) Obvious displacement between the landslide body and the surrounding environment, accompanied by cracks or differences in elevation; 4) The source area shows a brighter color, and the accumulation has transverse fissures and appears tongue-shaped; 5) Irregular stepped appearance in the accumulation body, with the terraces possibly transformed into residential areas or farmland.

4 Results and analysis

4.1 Landslide traces inventory

The landslide inventory serves as a crucial foundation for regional landslide risk assessment and prevention. Many scholars have conducted regional or individual landslide studies in Jianzha County (Yin et al., 2014; Guo et al., 2020b; Du et al., 2023; Tu et al., 2023). Although the study areas of these studies cover or partially cover Jianzha County, most have not established a complete landslide traces inventory that fully encompasses Jianzha County. Table 2 presents selected existing landslide records in Jianzha County. After objectively supplemented and validated by these records, the landslide inventory constructed in this study contains a total of 713 landslide traces (Figure 2). The total area of these landslides is 134.46 km^2. The total landslide area excluding the overlap area is 126.30 km^2, accounting for 7.37% of the study area. The average landslide area is approximately 0.19 km^2, with a minimum of 3,556 m^2 and a maximum of 11.13 km^2. It can be found that landslides mainly occur on the slopes of the relatively low-elevation ridges in the northeastern part of Jianzha County. These landslides are widely distributed in towns such as Kanbula, Jiajia, Cuozhou, Maketang, and Angla, with a predominance of large-scale landslides. In the southwest, where the altitude is relatively high, landslides are sparsely distributed.

4.2 Typical landslide display

In order to more intuitively display the landslides, several typical landslides were selected within the study area for display (Figure 3). It can be found that the predominant landslide type is loess landslide. The landslide boundary is easily identified based on the discontinuity in texture and shape between the deposits and the surrounding environment. The material movement along the slope is evident. The displacement between the landslide deposits and the boundary visually demonstrates the movement direction and shape of the landslide. Over time, traces of human activity become visible on the deposits. After reconstruction, roads and buildings of various sizes are distributed across the deposits. These typical landslide examples can clearly capture the landslide morphology and material movement traces, which is of great value for the study of regional landslide failure mechanisms.

4.3 Landslide density statistics

In order to quantitatively analyze the spatial distribution of landslides, landslide point density and area density are used to characterize the distribution and aggregation of landslides. After kernel density calculation with the search radius set to 2 km, the

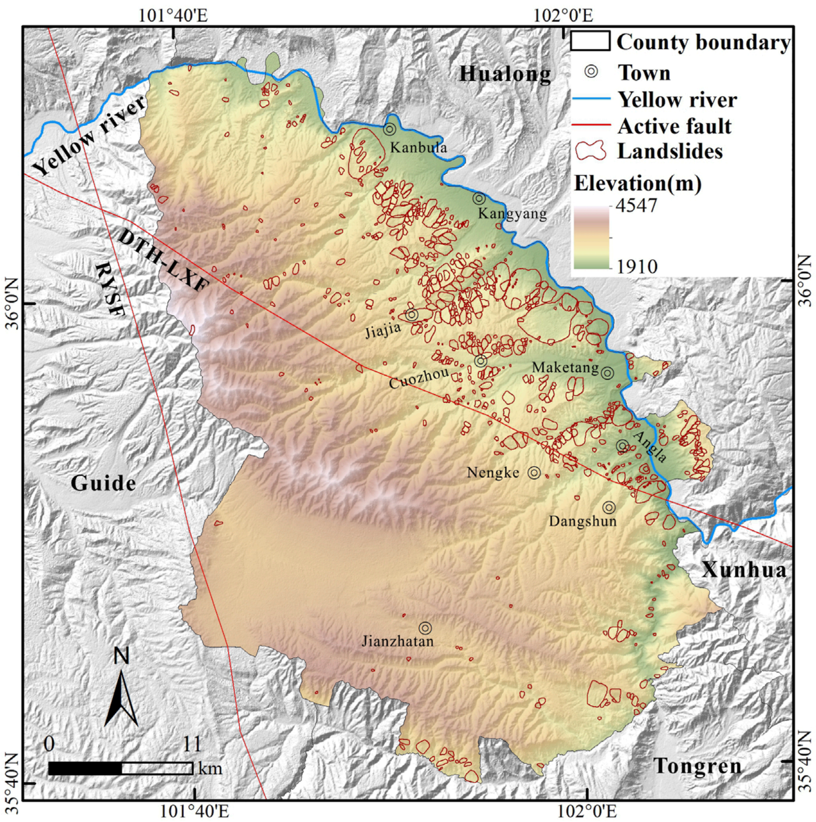

FIGURE 2
Spatial distribution map of landslide traces.

results are shown in Figure 4. High point density areas are primarily concentrated in the northeastern part of the study area (Figure 4A), with the maximum density reaching 5.69 km^{-2}. This indicates that landslides in these areas are numerically dominant. The maximum landslide area density is 98.0% (Figure 4B). High area density areas are different from high point density areas in distribution. For instance, landslide area density is more significant relative to point density in areas close to the Kanbula Town. This indicates that the landslides in this area tend to be larger in scale.

5 Discussion

5.1 Landslide scale and the completeness analysis

To explore the scale of landslides in Jianzha County, the cumulative landslide number was plotted against the landslide area in a double logarithmic coordinate system to show the relationship between them (Figure 5). Where N represents the number of landslides exceeding a given area, A. It can be observed that the majority of landslides have a scale smaller than 1×10^6 m^2, with only 14 landslides exceeding 1×10^6 m^2 in scale. The fitting formula for all landslides is $lgN(A) = -0.728\,lgA + 5.957$, with R^2=0.882. For landslides with an area larger than 1×10^5 m^2, the fitting formula is $lgN(A) = -1.210\,lgA + 8.552$, with R^2=0.99, indicating that these data are relatively complete. For landslides with an area smaller than 1×10^4 m^2, the curve exhibits a smoother trend, possibly due to the less distinct image change characteristics in the exposed loess areas, making them difficult to identify.

As shown in Figure 5, landslides with an area greater than 1×10^5 m^2 are fitted as $lgN(A) = -1.210\,lgA + 8.552$. In previous studies, this formula was often used in the statistics of coseismic landslide inventories to evaluate the completeness. For example, in the nearly complete coseismic landslide inventory established by Xu et al. (2014a) after the Wenchuan earthquake, landslides within a certain area are defined by the equation $lgN(A) = -2.0745\,lgA + 13$, and the landslides exhibit a rolling trend. Similarly, coseismic landslide inventories for the Minxian-Zhangxian earthquake (Xu et al., 2014b) and Maerkang earthquake (Chen et al., 2023) also show a similar trend, with the slopes and intercepts of the corresponding fitting equations are −1.341 and 6.02 (Minxian-Zhangxian earthquake) and −1.1052 and 5.7839 (Maerkang earthquake), respectively. Although the scale of landslides may vary due to different environmental conditions. However, it can be observed that whether it is the landslide traces inventory of this article or the coseismic landslide inventory, the landslides show a similar trend of change. In particular, in the work of establishing a landslide inventory with similar landslide scales, Li et al. (2022b) constructed a landslide traces inventory containing 3,757 landslides around the Baihetan Hydropower Station reservoir in China. The

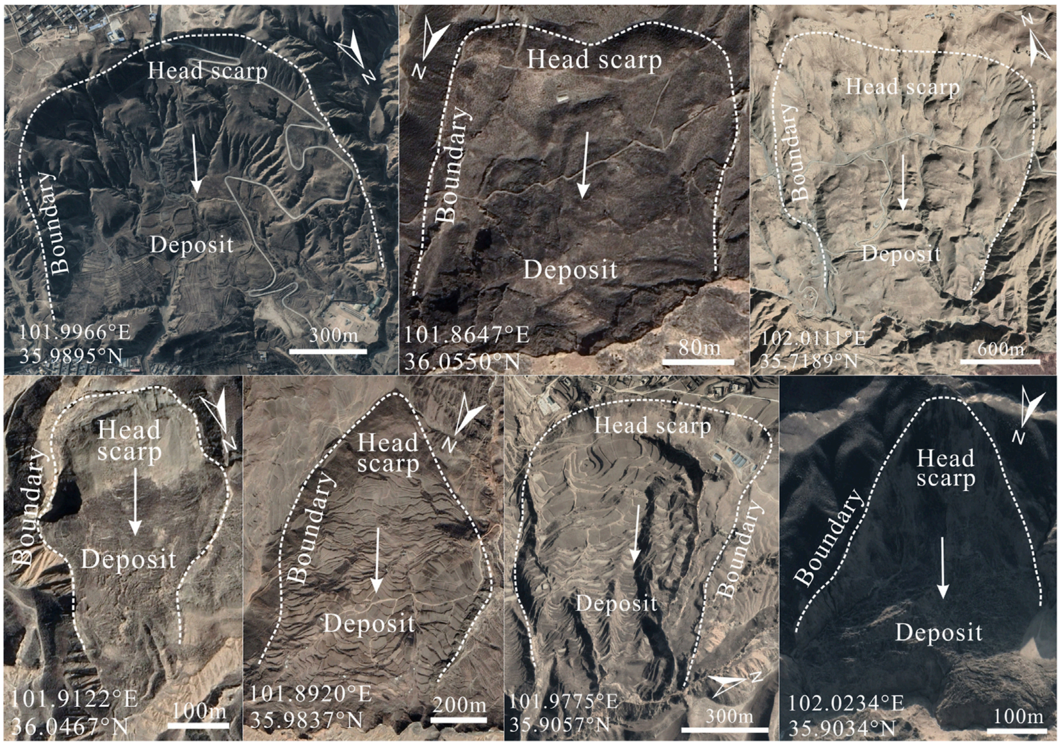

FIGURE 3
Display of seven typical landslide traces in the study area.

relationship between the cumulative number and area of landslides with an area greater than $1{\times}10^5$ m^2 is $lgN(A) = -1.275\,lgA + 6.26$. Upon comparison, this is very close to the results of this article, which also proves the completeness of our inventory to a certain extent. By comparing the completeness of landslide inventories in different categories, it is concluded that landslide inventories of the same category have more reference value than those of different categories.

5.2 Objective assessment of methods

A complete and detailed landslide inventory is of great significance for regional landslide research and risk management. The human-computer interaction visual interpretation method, as one of the primary approaches for establishing regional landslide inventory, possesses advantages that are irreplaceable by field investigation and automatic identification techniques (Guzzetti et al., 2012; Tian et al., 2019; Xu et al., 2020). While this study primarily relied on such a method to construct a relatively objective landslide traces inventory for Jianzha County, there are still some limitations. For small-scale landslides, due to the resolution limitations of satellite images, the coverage of topographic and geomorphic features, and the subjective factors from interpreters, it is inevitable that landslides with unclear identification characteristics will be missed. Compared with detailed field investigation, the visual interpretation method consumes less cost and time. Compared with automatic identification method, it is superior in accuracy and is currently a widely used method for identifying regional landslides (Cui et al., 2021; Li et al., 2022a; Sun et al., 2024). This method sacrifices some accuracy compared to field investigation, but greatly improves efficiency. Balancing the efficiency of automatic identification and the accuracy of field investigation is an exploratory and challenging task.

5.3 The importance of the landslide inventory

Landslide susceptibility refers to the probability of slope failure in a specific geological environment without considering triggering factors (Akgun, 2012; Nikoobakht et al., 2022). As a fundamental component, landslide inventory plays an indispensable role in landslide susceptibility assessment. It provides essential information about landslides, including the number, scale, location. Based on landslide inventory, one can select a single assessment method and specific influencing factors for landslide susceptibility assessment (Huangfu et al., 2021; Nanehkaran et al., 2021; Cemiloglu et al., 2023). Alternatively, one can choose several different assessment methods for comparative analysis to find the optimal results (Azarafza et al., 2021; Nanehkaran et al., 2022; Mao et al., 2024). With the development of landslide assessment, machine learning has demonstrated outstanding performance among many methods, gradually becoming the preferred approach for assessment (Nanehkaran et al., 2023). Based on susceptibility

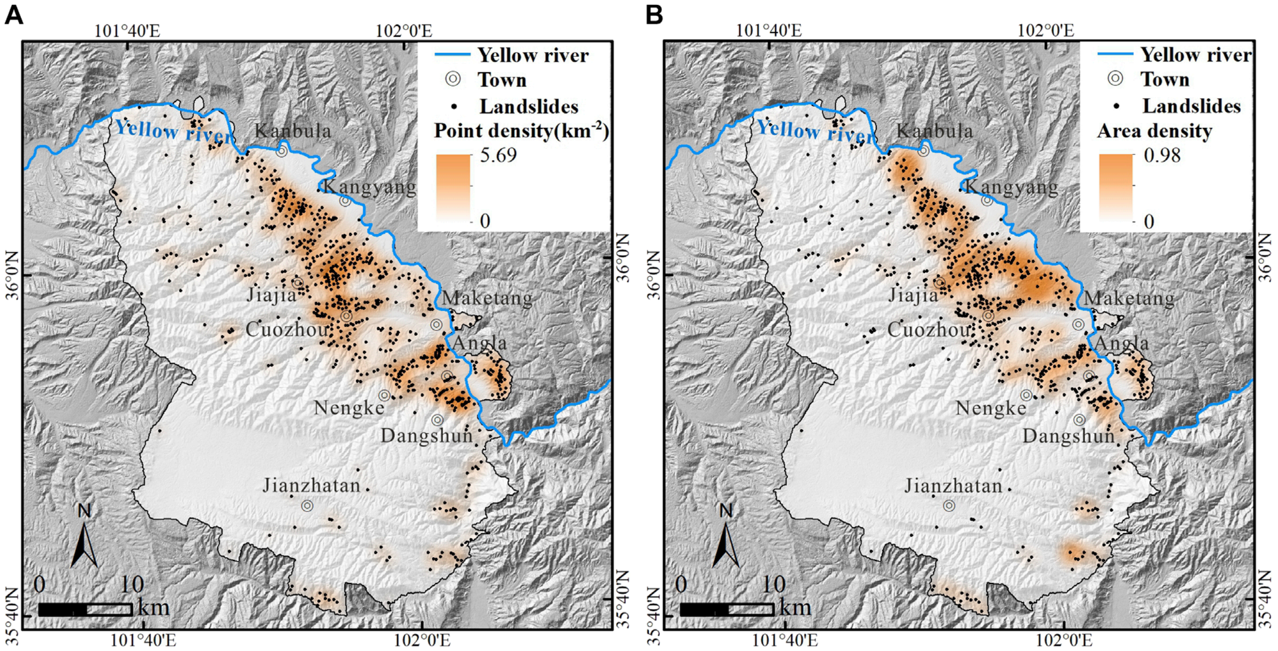

FIGURE 4
Landslide density map. **(A)** point density map; **(B)** area density map.

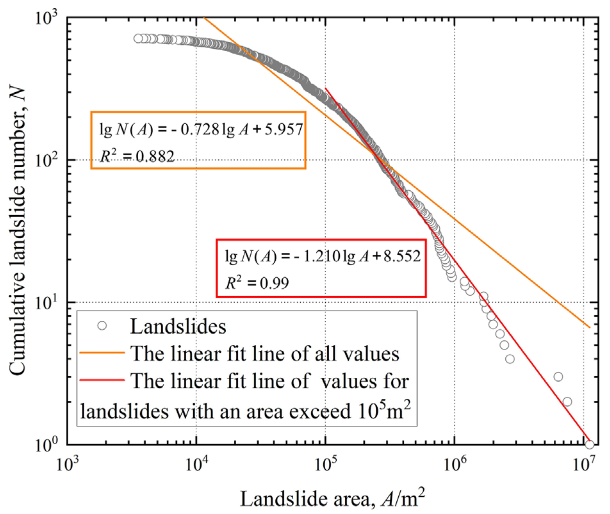

FIGURE 5
Curve depicting correlation between the cumulative landslide number and the landslide area.

assessment, triggering factors are added to evaluate landslide hazard, while carrier indicators are added for vulnerability assessment. Risk assessment is then performed by overlaying hazard and vulnerability. However, regardless of which assessment method is chosen and which landslide influencing factors are considered, the susceptibility assessment, hazard assessment, vulnerability assessment, and risk assessment all need to be based on landslide data. The landslide inventory can not only be used to validate the results obtained through predictive modeling, but also provide an important reference for exploring factors involved in the occurrence of new landslides. Many studies have been carried out on incomplete landslide inventories and updated the inventories, effectively enhancing the understanding of subsequent landslide development and assessment research. For example, the Hokkaido earthquake (Kasai and Yamada, 2019; Cui et al., 2021), Wenchuan earthquake (Dai et al., 2011; Xu et al., 2014a), and Jiuzhaigou earthquake (Tian et al., 2019; Sun et al., 2024). The work of compiling a complete and detailed landslide inventory is not only of great value and significance, but also has important supporting value for subsequent research on landslide failure mechanisms, landscape evolution, especially landslide susceptibility assessment.

6 Conclusion

This study established a landslide traces inventory in Jianzha County, Qinghai Province, China, and conducted a statistical analysis of their number, area, and density. A total of 713 landslides were identified, mainly loess landslides. The total area of landslides is 134.46 km^2, ranging in scale from 3556 m^2 to 11.13 km^2. The landslides are primarily concentrated in the low-elevation regions of the northeastern part of the study area. This inventory is more similar in scale and completeness to other loess landslide inventories. Furthermore, it is more complete and detailed than previous landslide traces records in Jianzha County. The study compiled the most complete and detailed landslide traces inventory in Jianzha County so far, which is of great significance to landslide scientific research. In future, relevant research on loess landslide development characteristics, failure mechanisms, susceptibility assessment and risk zoning can be conducted based on this landslide inventory.

Data availability statement

The raw data supporting the conclusion of this article will be made available by the authors, without undue reservation.

Author contributions

TL: Investigation, Visualization, Writing–original draft. CX: Conceptualization, Resources, Writing–review and editing. LL: Investigation, Writing–review and editing. JX: Investigation, Writing–review and editing.

Funding

The author(s) declare financial support was received for the research, authorship, and/or publication of this article. This work was supported by the National Institute of Natural Hazards, Ministry of Emergency Management of China (2023-JBKY-57) and the National Natural Science Foundation of China (42077259).

Acknowledgments

Deep thanks are extended to the reviewers for their beneficial review and valuable comments.

Conflict of interest

The authors declare that the research was conducted in the absence of any commercial or financial relationships that could be construed as a potential conflict of interest.

The author(s) declared that they were an editorial board member of Frontiers, at the time of submission. This had no impact on the peer review process and the final decision.

Publisher's note

References

Akgun, A. (2012). A comparison of landslide susceptibility maps produced by logistic regression, multi-criteria decision, and likelihood ratio methods: a case study at İzmir, Turkey. *Landslides* 9 (1), 93–106. doi:10.1007/s10346-011-0283-7

Azarafza, M., Azarafza, M., Akgün, H., Atkinson, P. M., and Derakhshani, R. (2021). Deep learning-based landslide susceptibility mapping. *Sci. Rep.* 11 (1), 24112. doi:10.1038/s41598-021-03585-1

Cemiloglu, A., Zhu, L., Mohammednour, A. B., Azarafza, M., and Nanehkaran, Y. A. (2023). Landslide susceptibility assessment for Maragheh County, Iran, using the logistic regression algorithm. *Land* 12 (7), 1397. doi:10.3390/land12071397

Chen, W., Chai, H., Zhao, Z., Wang, Q., and Hong, H. (2016). Landslide susceptibility mapping based on GIS and support vector machine models for the Qianyang county, China. *Environ. Earth Sci.* 75, 474. doi:10.1007/s12665-015-5093-0

Chen, Z., Huang, Y., He, X., Shao, X., Li, L., Xu, C., et al. (2023). Landslides triggered by the 10 June 2022 Maerkang earthquake swarm, Sichuan, China: spatial distribution and tectonic significance. *Landslides* 20, 2155–2169. doi:10.1007/s10346-023-02080-0

Craddock, W. H., Kirby, E., Harkins, N. W., Zhang, H., Shi, X., and Liu, J. (2010). Rapid fluvial incision along the Yellow River during headward basin integration. *Nat. Geosci.* 3 (3), 209–213. doi:10.1038/ngeo777

Crosby, C. J., Whitmeyer, S. J., De Paor, D. G., Bailey, J., and Ornduff, T. (2012). Lidar and Google Earth: simplifying access to high-resolution topography data. *Spec. Pap. Geol. Soc. Am.* 492, 37–47. doi:10.1130/2012.2492(03)

Cui, Y., Bao, P., Xu, C., Ma, S., Zheng, J., and Fu, G. (2021). Landslides triggered by the 6 September 2018 Mw6.6 Hokkaido, Japan: an updated inventory and retrospective hazard assessment. *Earth Sci. Inf.* 14, 247–258. doi:10.1007/s12145-020-00544-8

Cui, Y., Hu, J., Xu, C., Miao, H., and Zheng, J. (2022b). Landslides triggered by the 1970 Ms7.7 Tonghai earthquake in Yunnan, China: an inventory, distribution characteristics, and tectonic significance. *J. Mt. Sci.* 19 (6), 1633–1649. doi:10.1007/s11629-022-7321-x

Cui, Y., Hu, J., Zheng, J., Fu, G., and Xu, C. (2022a). Susceptibility assessment of landslides caused by snowmelt in a typical loess area in the Yining County, Xinjiang, China. *Q. J. Eng. Geol. Hydrogeology* 55 (1), qjegh2021–2024. doi:10.1144/qjegh2021-024

Cui, Y., Jin, J., Huang, Q., Yuan, K., and Xu, C. (2022c). A data-driven model for spatial shallow landslide probability of occurrence due to a typhoon in Ningguo City, Anhui Province, China. *Forests* 13 (5), 732. doi:10.3390/f13050732

Cui, Y., Yang, W., Xu, C., and Wu, S. (2023). Distribution of ancient landslides and landslide hazard assessment in the Western Himalayan Syntaxis area. *Front. Earth Sci.* 11, 1135018. doi:10.3389/feart.2023.1135018

Dai, F., Xu, C., Yao, X., Xu, L., Tu, X., and Gong, Q. (2011). Spatial distribution of landslides triggered by the 2008 Ms8.0 Wenchuan earthquake, China. *J. Asian Earth Sci.* 40 (4), 883–895. doi:10.1016/j.jseaes.2010.04.010

Deng, Q. (2007). *Map of active tectonics in China*. Beijing: Seismological Press. (In Chinese)

Du, J., Li, Z., Song, C., Zhu, W., Ji, Y., Zhang, C., et al. (2023). InSAR-based active landslide detection and characterization along the upper reaches of the Yellow River. *IEEE J. Sel. Top. Appl. Earth Observations Remote Sens.* 16, 3819–3830. doi:10.1109/jstars.2023.3263003

Fayne, J. V., Ahamed, A., Roberts-Pierel, J., Rumsey, A. C., and Kirschbaum, D. (2019). Automated satellite-based landslide identification product for Nepal. *Earth Interact.* 23 (3), 1–21. doi:10.1175/ei-d-17-0022.1

Froude, M. J., and Petley, D. N. (2018). Global fatal landslide occurrence from 2004 to 2016. *Nat. Hazards Earth Syst. Sci.* 18 (8), 2161–2181. doi:10.5194/nhess-18-2161-2018

Guo, X., Forman, S. L., Marin, L., and Li, X. (2018). Assessing tectonic and climatic controls for late quaternary fluvial terraces in Guide, Jianzha, and Xunhua basins along the Yellow River on the northeastern Tibetan plateau. *Quat. Sci. Rev.* 195, 109–121. doi:10.1016/j.quascirev.2018.07.005

Guo, X., Sun, Z., Lai, Z., Lu, Y., and Li, X. (2016). Optical dating of landslide-dammed lake deposits in the upper Yellow River, Qinghai-Tibetan Plateau, China. *Quat. Int.* 392, 233–238. doi:10.1016/j.quaint.2015.06.021

Guo, X., Wei, J., Lu, Y., Song, Z., and Liu, H. (2020a). Geomorphic effects of a dammed pleistocene lake formed by landslides along the upper Yellow River. *Water* 12 (5), 1350. doi:10.3390/w12051350

Guo, X., Wei, J., Song, Z., Lai, Z., and Yu, L. (2020b). Optically stimulated luminescence chronology and geomorphic imprint of Xiazangtan landslide upon the upper Yellow River valley on the northeastern Tibetan Plateau. *Geol. J.* 55 (7), 5498–5507. doi:10.1002/gj.3754

Guzzetti, F., Mondini, A. C., Cardinali, M., Fiorucci, F., Santangelo, M., and Chang, K.-T. (2012). Landslide inventory maps: new tools for an old problem. *Earth-Science Rev.* 112 (1-2), 42–66. doi:10.1016/j.earscirev.2012.02.001

Huang, Y., Xu, C., Li, L., He, X., Cheng, J., Xu, X., et al. (2022). Inventory and spatial distribution of ancient landslides in Hualong county, China. *Land* 12 (1), 136. doi:10.3390/land12010136

Huangfu, W., Wu, W., Zhou, X., Lin, Z., Zhang, G., Chen, R., et al. (2021). Landslide geo-hazard risk mapping using logistic regression modeling in Guixi, Jiangxi, China. *Sustainability* 13 (9), 4830. doi:10.3390/su13094830

Kasai, M., and Yamada, T. (2019). Topographic effects on frequency-size distribution of landslides triggered by the Hokkaido Eastern Iburi Earthquake in 2018. *Earth, Planets Space* 71 (1), 89–12. doi:10.1186/s40623-019-1069-8

Kirschbaum, D., Stanley, T., and Zhou, Y. (2015). Spatial and temporal analysis of a global landslide catalog. *Geomorphology* 249, 4–15. doi:10.1016/j.geomorph.2015.03.016

Lan, H. X., Zhou, C. H., Wang, L. J., Zhang, H. Y., and Li, R. H. (2004). Landslide hazard spatial analysis and prediction using GIS in the Xiaojiang watershed, Yunnan, China. *Eng. Geol.* 76 (1), 109–128. doi:10.1016/j.enggeo.2004.06.009

Li, L., Xu, C., Xu, X., Zhang, Z., and Cheng, J. (2021). Inventory and distribution characteristics of large-scale landslides in Baoji city, Shaanxi province, China. *ISPRS Int. J. Geo-Information* 11 (1), 10. doi:10.3390/ijgi11010010

Li, L., Xu, C., Yang, Z., Zhang, Z., and Lv, M. (2022a). An inventory of large-scale landslides in Baoji city, Shaanxi province, China. *Data* 7 (8), 114. doi:10.3390/data7080114

Li, L., Xu, C., Yao, X., Shao, B., Ouyang, J., Zhang, Z., et al. (2022b). Large-scale landslides around the reservoir area of Baihetan hydropower station in Southwest China: analysis of the spatial distribution. *Nat. Hazards Res.* 2 (3), 218–229. doi:10.1016/j.nhres.2022.07.002

Li, X., Guo, X., and Li, W. (2011). Mechanism of giant landslides from Longyangxia valley to Liujiaxia valley along upper Yellow River. *J. Eng. Geol.* 19 (4), 516–529 [in Chinese, with English summary].

Ma, X., Wang, L., Lv, B., and Ju, S. (2008). An investigation of geological hazards based on IRS-P^6 remote sensing data, Jianzha county, Qinghai province. *Northwest. Geol.* 41 (2), 93–100 [in Chinese, with English summary].

Mao, Y., Li, Y., Teng, F., Sabonchi, A. K. S., Azarafza, M., and Zhang, M. (2024). Utilizing hybrid machine learning and soft computing techniques for landslide susceptibility mapping in a Drainage Basin. *Water* 16 (3), 380. doi:10.3390/w16030380

Milledge, D. G., Bellugi, D. G., Watt, J., and Densmore, A. L. (2022). Automated determination of landslide locations after large trigger events: advantages and disadvantages compared to manual mapping. *Nat. Hazards Earth Syst. Sci.* 22 (2), 481–508. doi:10.5194/nhess-22-481-2022

Nanehkaran, Y. A., Chen, B., Cemiloglu, A., Chen, J., Anwar, S., Azarafza, M., et al. (2023). Riverside landslide susceptibility overview: leveraging artificial neural networks and machine learning in accordance with the United Nations (UN) sustainable development goals. *Water* 15 (15), 2707. doi:10.3390/w15152707

Nanehkaran, Y. A., Licai, Z., Chen, J., Azarafza, M., and Yimin, M. (2022). Application of artificial neural networks and geographic information system to provide hazard susceptibility maps for rockfall failures. *Environ. Earth Sci.* 81 (19), 475. doi:10.1007/s12665-022-10603-6

Nanehkaran, Y. A., Mao, Y., Azarafza, M., Kockar, M. K., and Zhu, H.-H. (2021). Fuzzy-based multiple decision method for landslide susceptibility and hazard assessment: a case study of Tabriz, Iran. *Geomechanics Eng.* 24 (5), 407–418. doi:10.12989/gae.2021.24.5.407

Nikoobakht, S., Azarafza, M., Akgün, H., and Derakhshani, R. (2022). Landslide susceptibility assessment by using convolutional neural network. *Appl. Sci.* 12 (12), 5992. doi:10.3390/app12125992

Peng, D., Xu, Q., Qi, X., Fan, X., Dong, X., Li, S., et al. (2016). Study on early recognition of loess landslides based on field investigation. *Int. J. Georesources Environment-IJGE Former. Int'l J Geohazards Environ.* 2 (2), 35–52. doi:10.15273/ijge.2016.02.006

Peng, J., Lan, H., Qian, H., Wang, W., Li, R., Li, Z., et al. (2020). Scientific research framework of livable Yellow River. *J. Eng. Geol.* 28 (2), 189–201 [in Chinese, with English summary].

Petley, D. (2012). Global patterns of loss of life from landslides. *Geology* 40 (10), 927–930. doi:10.1130/g33217.1

Piacentini, D., Troiani, F., Daniele, G., and Pizziolo, M. (2018). Historical geospatial database for landslide analysis: the catalogue of landslide occurrences in the Emilia-Romagna region (CLOCkER). *Landslides* 15 (4), 811–822. doi:10.1007/s10346-018-0962-8

Piralilou, S. T., Shahabi, H., and Pazur, R. (2021). Automatic landslide detection using bi-temporal sentinel 2 imagery. *GI_Forum* 9, 39–45. doi:10.1553/giscience2021_01_s39

Qiu, H., Cui, Y., Yang, D., Pei, Y., Hu, S., Ma, S., et al. (2019). Spatiotemporal distribution of nonseismic landslides during the last 22 years in Shaanxi province, China. *ISPRS Int. J. Geo-Information* 8 (11), 505. doi:10.3390/ijgi8110505

Rabby, Y. W., and Li, Y. (2019). An integrated approach to map landslides in Chittagong Hilly Areas, Bangladesh, using Google Earth and field mapping. *Landslides* 16 (3), 633–645. doi:10.1007/s10346-018-1107-9

Shao, X., Ma, S., Xu, C., Shen, L., and Lu, Y. (2020). Inventory, distribution and geometric characteristics of landslides in Baoshan city, Yunnan province, China. *Sustainability* 12 (6), 2433. doi:10.3390/su12062433

Sun, J., Shao, X., Feng, L., Xu, C., Huang, Y., and Yang, W. (2024). An essential update on the inventory of landslides triggered by the Jiuzhaigou Mw6. 5 earthquake in China on 8 August 2017, with their spatial distribution analyses. *Heliyon* 10 (2), e24787. doi:10.1016/j.heliyon.2024.e24787

Tian, Y., Xu, C., Ma, S., Xu, X., Wang, S., and Zhang, H. (2019). Inventory and spatial distribution of landslides triggered by the 8th August 2017 Mw 6.5 Jiuzhaigou earthquake, China. *J. Earth Sci.* 30 (1), 206–217. doi:10.1007/s12583-018-0869-2

Tu, K., Ye, S., Zou, J., Hua, C., and Guo, J. (2023). InSAR displacement with high-resolution optical remote sensing for the early detection and deformation analysis of active landslides in the upper Yellow River. *Water* 15 (4), 769. doi:10.3390/w15040769

Vecchiotti, F., Tilch, N., and Kociu, A. (2021). The use of TERRA-ASTER satellite for landslide detection. *Geosciences* 11 (6), 258. doi:10.3390/geosciences11060258

Wang, L., Qiu, H., Zhou, W., Zhu, Y., Liu, Z., Ma, S., et al. (2022). The post-failure spatiotemporal deformation of certain translational landslides may follow the pre-failure pattern. *Remote Sens.* 14 (10), 2333. doi:10.3390/rs14102333

Wu, Y., Li, W., Liu, P., Bai, H., Wang, Q., He, J., et al. (2016). Application of analytic hierarchy process model for landslide susceptibility mapping in the Gangu County, Gansu Province, China. *Environ. Earth Sci.* 75, 422. doi:10.1007/s12665-015-5194-9

Xu, C. (2015). Preparation of earthquake-triggered landslide inventory maps using remote sensing and GIS technologies: principles and case studies. *Geosci. Front.* 6 (6), 825–836. doi:10.1016/j.gsf.2014.03.004

Xu, C., Xu, X., and Shyu, J. B. H. (2015). Database and spatial distribution of landslides triggered by the Lushan, China Mw6.6 earthquake of 20 April 2013. *Geomorphology* 248, 77–92. doi:10.1016/j.geomorph.2015.07.002

Xu, C., Xu, X., Shyu, J. B. H., Zheng, W., and Min, W. (2014b). Landslides triggered by the 22 July 2013 Minxian–Zhangxian, China, Mw5.9 earthquake: inventory compiling and spatial distribution analysis. *J. Asian Earth Sci.* 92, 125–142. doi:10.1016/j.jseaes.2014.06.014

Xu, C., Xu, X., Yao, X., and Dai, F. (2014a). Three (nearly) complete inventories of landslides triggered by the May 12, 2008 Wenchuan Mw7.9 earthquake of China and their spatial distribution statistical analysis. *Landslides* 11, 441–461. doi:10.1007/s10346-013-0404-6

Xu, X., and Xu, C. (2021). Natural Hazards Research: an eternal subject of human survival and development. *Nat. Hazards Res.* 1 (1), 1–3. doi:10.1016/j.nhres.2020.12.003

Xu, Y., Allen, M. B., Zhang, W., Li, W., and He, H. (2020). Landslide characteristics in the Loess Plateau, northern China. *Geomorphology* 359, 107150. doi:10.1016/j.geomorph.2020.107150

Yin, Z., Qin, X., and Zhao, W. (2014). "Characteristics of landslides from sigou gorge to lagan gorge in the upper reaches of Yellow River. Landslide Science for a Safer Geoenvironment: vol. 1," in *The international programme on landslides (IPL)* (Springer).

Yin, Z., Qin, X., Zhao, W., and Wei, G. (2013a). Characteristics of landslides in upper reaches of Yellow River with multiple data of remote sensing. *J. Eng. Geol.* 21 (5), 779–787 [in Chinese, with English summary].

Yin, Z., Wei, G., Qi, X., and Zhou, C. (2013b). Spatial and temporal characteristics of landslides and there response to climatic change from Sigou to Lagan gorges in upper reaches of Yellow River. *J. Eng. Geol.* 21 (1), 129–137 [in Chinese, with English summary].

Yin, Z., Wei, G., Qin, X., Li, W., and Zhao, W. (2021). Research progress on landslides and dammed lakes in the upper reaches of the Yellow River, northeastern Tibetan Plateau. *Earth Sci. Front.* 28 (2), 46–57 [in Chinese, with English summary].

Zhang, F., and Huang, X. (2018). Trend and spatiotemporal distribution of fatal landslides triggered by non-seismic effects in China. *Landslides* 15 (8), 1663–1674. doi:10.1007/s10346-018-1007-z

Zhang, P., Xu, C., Ma, S., Shao, X., Tian, Y., and Wen, B. (2020a). Automatic extraction of seismic landslides in large areas with complex environments based on deep learning: an example of the 2018 Iburi earthquake, Japan. *Remote Sens.* 12 (23), 3992. doi:10.3390/rs12233992

Zhang, Z., Wang, T., and Wu, S. (2020b). Distribution and features of landslides in the tianshui basin, northwest China. *J. Mt. Sci.* 17 (3), 686–708. doi:10.1007/s11629-019-5595-4

Zhao, B., Wang, Y., Chen, M., Luo, Y., Liang, R., and Li, J. (2019). Typical characteristics of large-scale landslides in the transition belt between the Qinghai-Tibet Plateau and the Loess Plateau. *Arabian J. Geosciences* 12, 470. doi:10.1007/s12517-019-4612-9